Detailed Heat Transfer Coefficient Measurements and Thermal Analysis at Engine Conditions of a Pedestal With Fillet Radii

Z. Wang

P. T. Ireland

T. V. Jones

Department of Engineering Science,
University of Oxford,
Oxford, United Kingdom

The heat transfer coefficient over the surface of a pedestal with fillet radii has been measured using thermochromic liquid crystals and the transient heat transfer method. The tests were performed at engine representative Reynolds numbers for a geometry typical of those used in turbine blade cooling systems. The heat conduction process that occurs in the engine was subsequently modeled numerically with a finite element discretization of the solid pedestal. The measured heat transfer coefficients were used to derive the exact boundary conditions applicable to the engine. The temperature field within the pedestal, calculated using the correct heat transfer coefficient distribution, is compared to that calculated using an area-averaged heat transfer coefficient. Metal temperature differences of 90 K are predicted across the blade wall.

Introduction

Short pin-fin and pin-fin arrays are frequently used in turbine blade internal cooling systems to enhance cooling and stiffen the structure. The present work has shown that a knowledge of the detailed heat transfer coefficient distribution is required to predict the cooling effect of such devices accurately. The heat flow process has been numerically modeled at typical engine conditions with the detailed heat transfer distribution measured by the transient heat transfer method being used as the thermal boundary conditions.

One outcome of the blade manufacturing process is that pin-fins found in internal cooling passages blend into the passage wall instead of joining the end wall to form an abrupt edge (Fig. 1). Large-scale (100 times engine size) perspex models were used in the present study to represent the engine pedestal geometry accurately. Previous researchers (Ireland and Jones, 1986; Metzger et al., 1986; Van Fossen, 1982; Zukauskas, 1972) have considered pin-fins without fillet radii. The effect of this simplification in model geometry on the detailed distribution of heat transfer coefficient has not been assessed. Chyu (1990) used the mass to heat transfer analogy method to measure the difference in the average mass transfer from arrays of pin fins with and without fillet radii. He concluded that the average Sherwood number on the pin fin surface for a staggered array was less with fillet radii than for straight pin fins. The presence of fillet radii had little effect on the Sherwood number for in-line configurations. The present work has measured local values of h and enables the extent of the effect of the blend radius to be estimated.

Prevous experimental studies of heat transfer to pin-fins have been performed without representing the temperature distribution in the pedestal material caused by the finite blade conductivity. Such tests have employed highly conductive models or have applied the mass to heat transfer analogy. Preliminary estimates of the temperature change across an engine pin fin indicated that the pin fin temperature difference could be of the order of 10–20 percent of the coolant to free-stream cooling potential. This value of the expected temperature change is typical of those occurring in engine cooling passages as discussed by Holland (1991) who gives a typical Biot number for a high-pressure turbine of 0.2. The recently acquired knowledge of the local heat transfer coefficient distribution has enabled the temperature change through the conducting blade material to be properly accounted for as reported below.

Heat Transfer Coefficient Measurements

Experimental Method. The distribution of heat transfer coefficient in this study was measured by a transient heat transfer liquid crystal method (Byerley et al., 1992; Shen et al., 1991). Thermochromic liquid crystals that exhibit color display over a certain temperature range are used as a full cover surface thermometer. The liquid crystal compounds are encapsulated in spheres of approximately 10 μm diameter and sprayed onto the model surface to form a thermally thin layer (Jones et al., 1992). In each test, the model temperature is initially uniform at room temperature. The experiment

Contributed by the International Gas Turbine Institute and presented at the 38th International Gas Turbine and Aeroengine Congress and Exposition, Cincinnati, Ohio, May 24–27, 1993. Manuscript received at ASME Headquarters March 17, 1993. Paper No. 93-GT-329. Associate Technical Editor: H. Lukas.

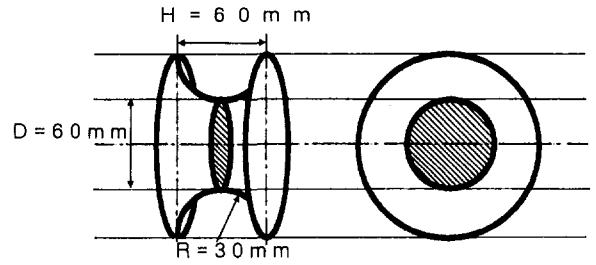

Fig. 1 Large-scale model of a pedestal with fillet radii

commences when the model is suddenly exposed to a flow of air at a temperature higher than the liquid crystal color change temperature. As the experiment proceeds, the liquid crystal coating on the model surface displays color when the local surface reaches the liquid crystal color change temperature. The surface temperature rise is a function of the local heat transfer coefficient given by the following equation:

$$\theta = 1 - \exp \beta^2 erfc\, \beta \tag{1}$$

where

$$\beta = \frac{h\sqrt{t}}{\sqrt{\rho ck}} \tag{2}$$

and

$$\theta = \frac{T_s - T_{\text{init}}}{T_{\text{gas}} - T_{\text{init}}} \tag{3}$$

T_{init} and T_{gas} are the initial temperature and the gas temperature. T_s corresponds to the liquid crystal color change temperature and t is the time at which the color display appears at the location where h is measured. T_{init} and T_{gas} are measured during the experiment and the local heat transfer coefficient can be calculated from the equation above. In this study, the color change times were found using a frame grabber fitted to a PC and the intensity history analysis method detailed by Wang et al. (1990) and Wang (1991) was used to process the data.

Experimental Apparatus. The experimental apparatus is shown in Fig. 2. The air from the heater is initially directed through the bypass that takes the same flow rate as that passing through the test section during the experiment. The test commences when the hot flow is switched by two fast-acting valves through the test section (shown by the solid arrows in Fig. 2). The test section is a high-aspect-ratio channel (60 × 600 × 1500 mm). The pedestal with fillet radii is placed on the duct centerline sufficiently far from the duct inlet for the flow to be fully developed. The pedestal spans the channel shortest dimension. The midspan ($z/H = 0.5$) diameter of the pedestal at 60 mm is the same as the channel width, H, and the radius of the fillets is half of the pedestal

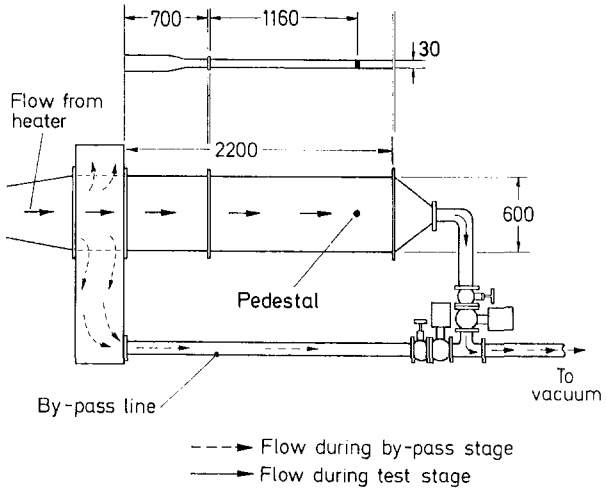

Fig. 2 Experimental apparatus

length. There is no straight section on the pedestal. The channel and the pedestal were manufactured from perspex. A liquid crystal coating that displayed color over two distinct temperature ranges was used in this work to calculate h twice at each selected location. A thin layer of black ink was applied on top of the liquid crystal film to eliminate transmitted light. The data presented below are the average of these two values. The experimental uncertainty was calculated, following the approach of Byerley (1992) and Ireland (1987), as being less than 7 percent.

Heat Transfer Coefficient Results. The dimensionless heat transfer coefficient on the channel wall at a location remote from the pedestal is plotted in Fig. 3. The experimental data are very close to the prediction from Kays and Crawford (1980) for fully developed channel flow. The measured heat transfer coefficients divided by the base level are depicted as contours in Fig. 4. The locations at which the crystal color change times were evaluated are indicated by the asterisks. There are about 120 data points on the pedestal surface and 80 points distributed over the end wall. This measurement density was sufficient to resolve all the features in the heat transfer coefficient distribution from the recorded video data.

The interpolated enhancement factor distributions (projected onto the channel wall) at different Reynolds numbers are shown in Fig. 5. It can be seen that the heat transfer is enhanced above the duct level on both the pedestal and the end wall surface. Similar regions of high convective transfer near the cylinder to wall junction have been measured using the mass transfer method of Goldstein and Karni (1984) and Sparrow et al. (1984). The highest heat transfer is found at

Nomenclature

A = area of the pedestal base
d = pedestal diameter in local plane
D = pedestal diameter (on $z/H = 0.5$ plane)
Fr = Frossling number
h = heat transfer coefficient
H = pedestal length
k = thermal conductivity
Nu = Nusselt number
Q = heat flow through extended pedestal base
$Q1$ = reference (flat wall) heat flow
Re = Reynolds number
t = time
T = temperature
u = velocity
x = distance upstream of pedestal centerline
z = distance normal to channel wall
β = dimensionless time
η = fin efficiency
θ = dimensionless surface temperature
ν = kinematic viscosity
β = dimensionless time
$\sqrt{\rho ck}$ = thermal product of perspex

Subscripts

CL = centerline plane ($z = H/2$)
cool = coolant
ext = external
gas = gas
init = initial
max = maximum
mb = mixed bulk
s = surface
z = in plane at distance z from channel wall

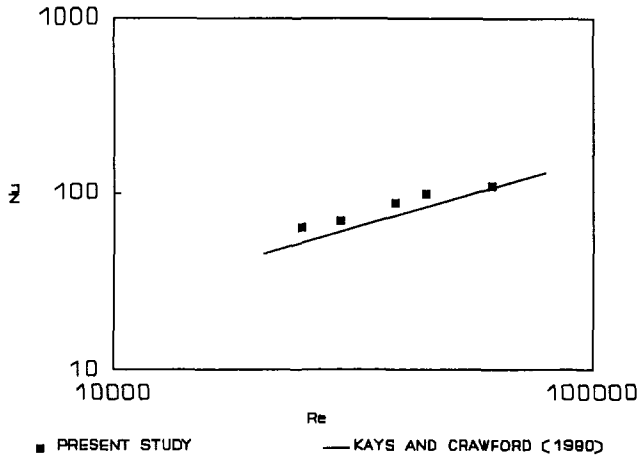

Fig. 3 Measured channel Nusselt number as a function of Reynolds number

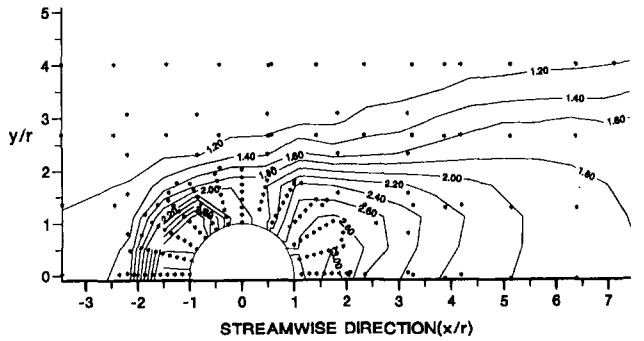

Fig. 4 Heat transfer enhancement factor measured over the pedestal surface

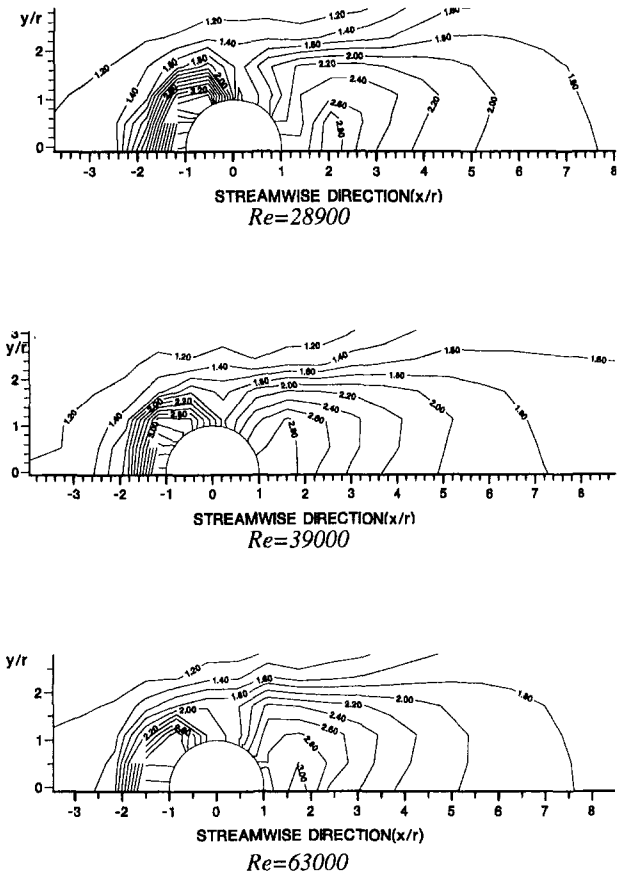

Fig. 5 Interpolated heat transfer coefficient distribution over the pedestal surface

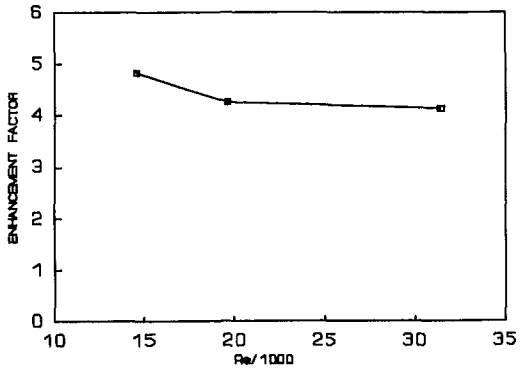

Fig. 6 Stagnation point heat transfer enhancement factor as a function of pedestal Reynolds number

the front stagnation point. The reduction in enhancement factor at the stagnation point with Reynolds number (Fig. 6), would be expected if the boundary layer on the front surface of the pedestal is laminar. The heat transfer coefficient under these conditions is proportional to the square root of Reynolds number while for the turbulent channel flow, h varies with Reynolds number to the 0.73 (Ireland, 1987).

On the end wall, the heat transfer is lower than on the pedestal and, at the side, is within 20 percent of the base level at a distance of 1.5D from the pedestal centerline. For comparison the heat transfer enhancement on the end wall adjacent to a straight pedestal ($H/D = 1$) (from Ireland, 1987) at similar Reynolds numbers is shown in Fig. 7. Figure 8 shows the heat transfer coefficient plotted against distance from the pedestal along the upstream line of channel symmetry. In the case of the straight pedestal, this line starts ($x/D = 0.5$) at the cylinder to end wall junction. The same coordinate on the blended pedestal is at the stagnation point on the pedestal surface ($z/H = 0.5$). It is of interest to note that the heat transfer coefficient at the root of the straight pedestal is much higher than at the front of the filleted pedestal. The peak at the root of the straight pedestal has been shown (Ireland, 1987) to be close to the attachment point of the main horseshoe vortex. One other significant difference between the two heat transfer distributions is that, at about $x/D = 0.7$, the heat transfer coefficient distribution for the straight pedestal exhibits a local minimum and local maximum. This feature, marked as X in Fig. 7, appears as the kinks in the otherwise smooth contours of enhancement factor. This locally high heat transfer ring was interpreted as being caused by a second (separation) vortex parallel to the main horseshoe vortex. The trough in heat transfer was associated with the separation vortex, which resides between the main and the separation vortices. The absence of similar kinks in Fig. 5 together with Fig. 8 indicate that the vortex structure has been modified by the presence of the fillet radius. The heat transfer distribution in the fillet pedestal case is shown in Fig. 8 monotonically decreasing in the upstream direction. However, at x/D is 0.7, the heat transfer coefficient decreases at a lesser rate with distance. The flow phenomenon that causes this change in gradient has not been resolved. It will be shown below, that the heat transfer enhancement at the front fillet radius appears to be mainly caused by attachment of the flow on the stagnation line and the growth of a new boundary layer.

Over the front of the pedestal where the boundary layer would be expected to be laminar, the Nusselt number should increase with the square root of Reynolds number. For a straight cylinder, the Reynolds number and Nusselt number

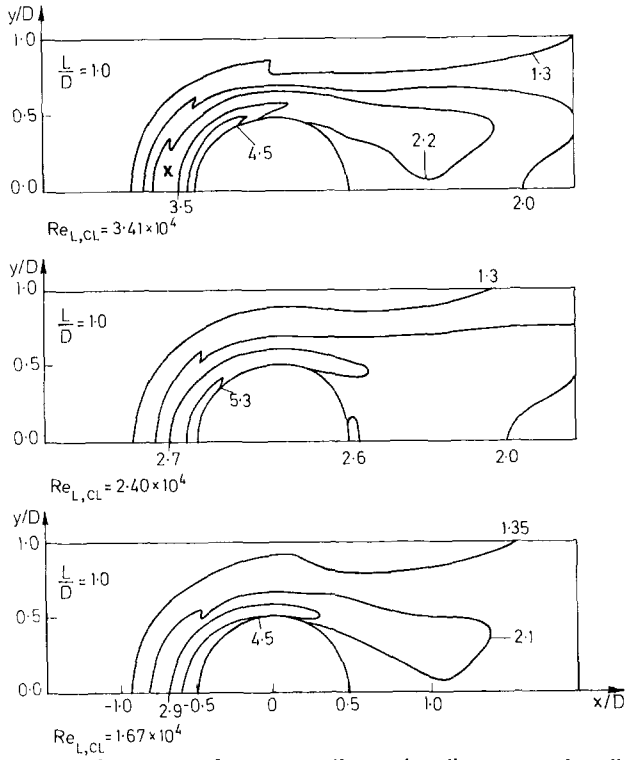

Fig. 7 Enhancement factor over the end wall near a prismatic pedestal after Ireland (1987)

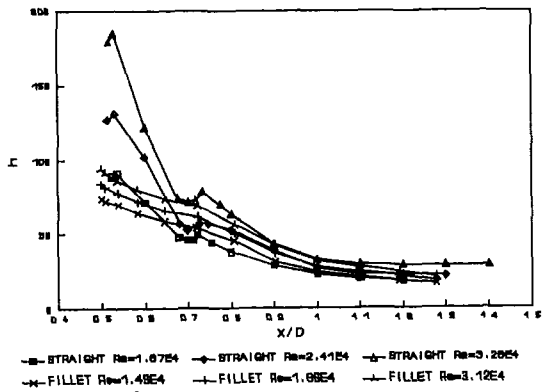

Fig. 8 (W/m²K) on a line leading upstream of the pedestal as a function of distance from the pedestal center

would be based on the cylinder diameter. In the case of the pedestal with fillet radii, it is of interest to consider the Nusselt number divided by the square root of Reynolds number (the Frossling number)

$$\mathrm{Fr} = \frac{\mathrm{Nu}}{\sqrt{\mathrm{Re}}} = \frac{h\sqrt{d\nu}}{k\sqrt{u_{CL}}} \tag{4}$$

over the front of the pedestal. The diameter most appropriate to add value to comparisons with other data is not immediately obvious.

The Frossling number, based on the midspan diameter D, at different Reynolds numbers and in a midspan plane is plotted as a function of angle from the leading edge in Fig. 9. The insensitivity of Fr to Reynolds number under the laminar boundary layer is apparent. In this figure, the Reynolds number is based on the diameter of the midspan circumference. Compared to the results obtained on both long pedestals and short straight pedestals, the heat transfer distribution at the midspan of the blended pedestal is similar and the levels are comparable. The stagnation point value is higher than

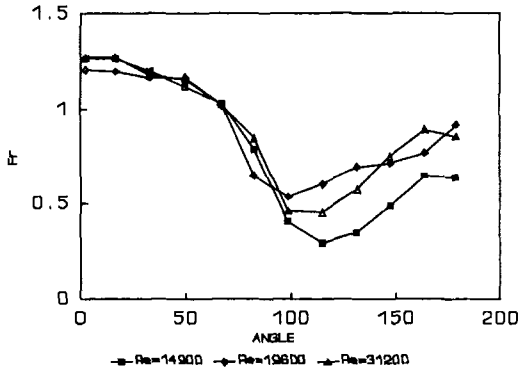

Fig. 9 Fr (based on D) around the midspan of the pedestal with fillet radii

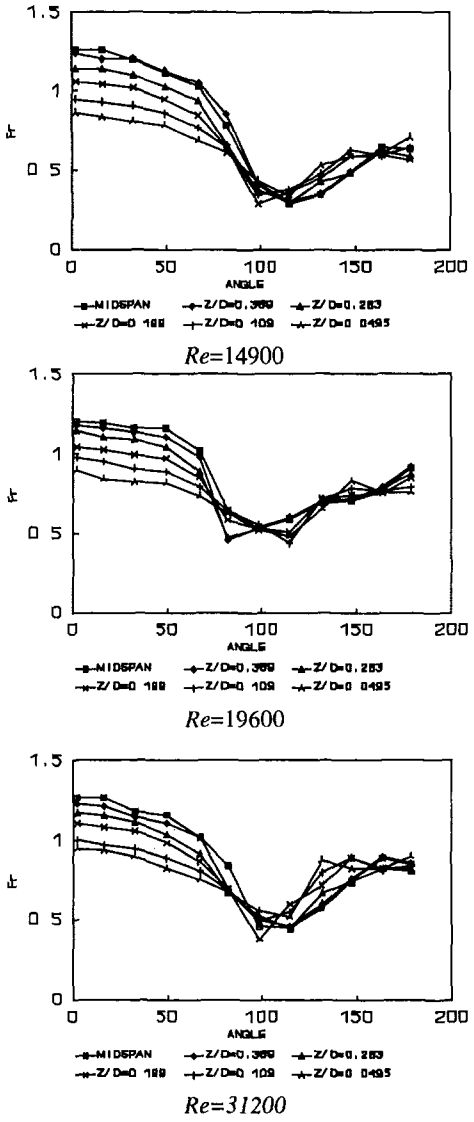

Fig. 10 Fr (based on D) around planes at different distances from the channel wall

the theoretical straight cylinder value of 0.99. A similar increase was observed on a straight pedestal in the same channel (Ireland, 1987) and was thought to be due to turbulence.

The Frossling number distribution around circular planes aligned parallel to, but at different distances from, the channel wall is presented in Fig. 10. It can be seen that the heat

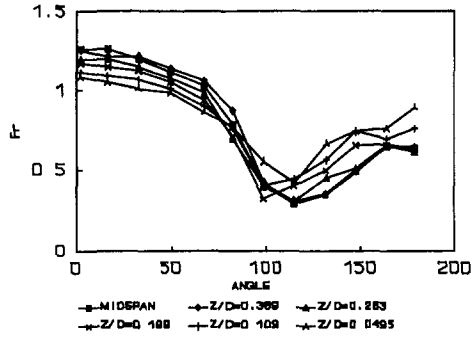

Re=14900

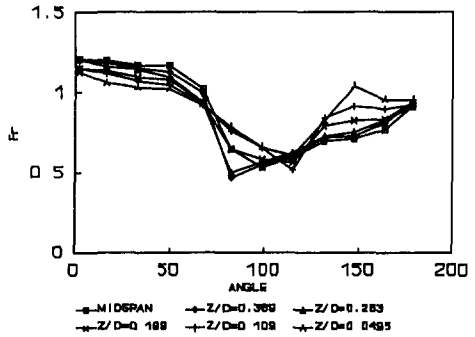

Re=19600

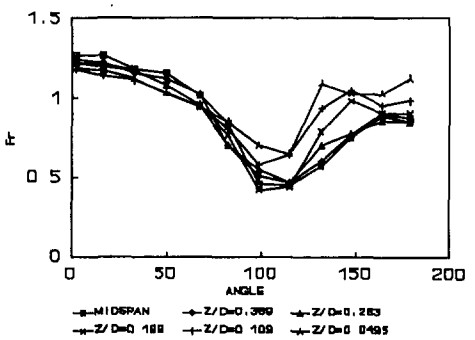

Re=31200

Fig. 11 Fr based on local plane diameter

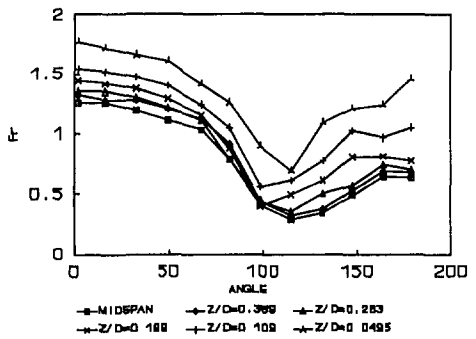

Re=14900

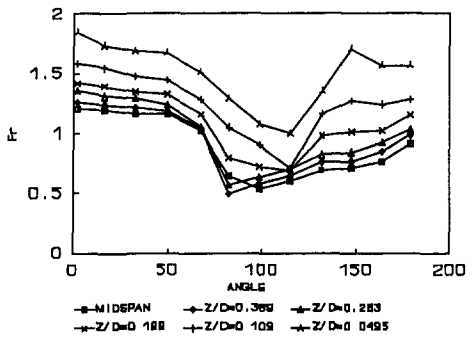

Re=19600

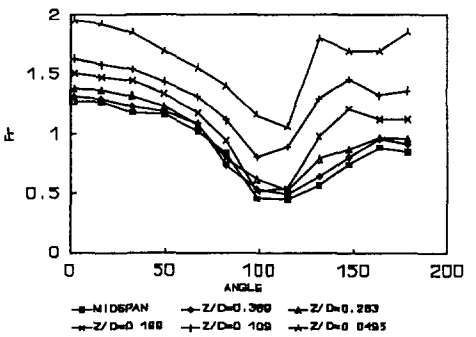

Re=31200

Fig. 12 Fr based on local plane diameter with factors applied to account for upstream gas temperature and velocity profiles

transfer coefficients decrease toward the endwall. There are three main differences between the flow around the midspan plane and that closer to the wall. Close to the wall:

(*a*) the local circle has a bigger diameter;
(*b*) the approach flow is lower in the channel boundary layer where the air stream is slower and cooler;
(*c*) the flow is no longer two dimensional.

To investigate (*a*), the Frossling number was then recalculated for each plane, using the value of diameter, d, local to that plane, Fig. 11. The uniform Fr at the front of the pedestal indicates that the flow can be treated as essentially two dimensional in this region. Strong secondary flows are either not present over most of the pedestal front or have very little effect on heat transfer levels. In this figure, the velocity used to calculate Fr is u_{CL}. Measurements confirmed that the channel velocity profile and temperature profile at a distance $2.6D$ ahead of the pedestal were fully developed. The effect of allowing for the upstream velocity and temperature profiles was also investigated. If the flow around the front of the pedestal does not migrate in the z direction and the flow around any circular slice of the pedestal is thus two dimensional, Fr based on local values of diameter, upstream temperature, and upstream velocity would collapse. The data were divided by a factor $(z/0.5H)^{1.5}$, which accounts for the seventh power law velocity and temperature profiles. The agreement between data from different planes can be seen to worsen (Fig. 12). The fact that the centerline velocity and temperature are the better values to collapse the Fr data is of interest and suggests that most of the front of the pedestal is swept by the flow originating remote from the channel wall.

At around 90 deg from the upstream line of symmetry, a narrow region of low heat transfer is found on the pedestal, which aligns with the pedestal axis and extends some distance from the midspan plane. This is caused by a region of separated flow, which has been identified many times on straight infinitely long cylinders. Interestingly the zone of low heat transfer extends almost to the end of the fillet where the surface is close to flat.

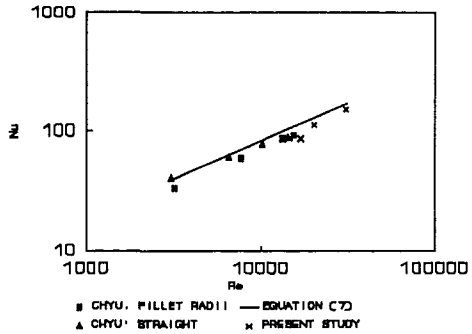

Fig. 13 Average Nu based on mixed bulk gas temperature as a function of Re based on mixed bulk channel velocity

Behind the pedestal, at about 150 deg, near to the junction between the fillet radius and the end wall, a high heat transfer region can be seen. This is the result of the reattachment of the horseshoe vortex to the surface. The divergence of the heat transfer contours downstream of this position is due to the gradual expansion of the horseshoe vortex leading to a double lobe shaped (only half is shown) enhancement region, which is similar to that found behind straight pedestals. In general, the region where heat transfer is enhanced behind the pedestal with fillet radii is wider and longer compared to a straight cylinder with a diameter the same as the midspan diameter. This would be expected since the pedestal with fillet radii presents more blockage. Extra heat transfer enhancement is obtained at the expense of increased pressure drop (Wang, 1991).

The heat transfer coefficient averaged over the surface of the pedestal with fillet radii is compared to the results of Chyu (1990) in Fig. 13. The data from this reference were taken from the first row of staggered arrays of straight pedestals and pedestals with fillet radii. The average Nusselt number has been calculated from the Sherwood number by multiplying by a factor of 0.6, which is the ratio of Schmidt number to Prandtl number raised to 0.4. Reynolds number used in the plot is based on the local mixed bulk velocity ahead of the pedestal and the

$$\mathrm{Re} = \frac{U_{mb} D}{\nu} \tag{6}$$

pedestal diameter. Account has been taken of the difference in the minimum area and the channel area in determining Re for the first row data from (1989). Chyu's data reveals slightly lower Nusselt numbers for the blended pedestal compared to the straight pedestal. A similar reduction in average value was found for the heat transfer data. The data from the present work (the crosses) have been calculated based on the mixed bulk air temperature. The line is from a correlation (Eq. (7)) for pedestal average mixed bulk Nusselt number established for straight pedestals in isolated and row configurations from Ireland (1987).

$$\mathrm{Nu} = 0.282\ \mathrm{Re}^{0.617} \tag{7}$$

It can be seen that the convective transfer data for the pedestal with fillet radii is lower than the straight cylinder correlation.

Conduction Analysis

In simple thermal analysis of pedestals no account is taken of the temperature variation through the body of the pedestal. The pedestal is essentially treated as having infinite thermal conductivity and an average value of the heat transfer coefficient is assumed to act over the surface of the pedestal. If the pedestal has a length-to-diameter ratio greater than 0.5, then

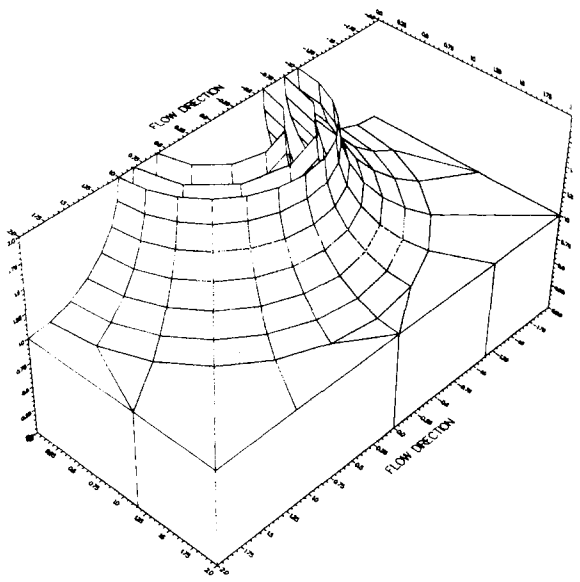

Fig. 14 Finite element calculation domain

the wetted area is increased. The change in area exposed to the flow is easily accounted for by defining an effective heat transfer coefficient (Brigham and Van Fossen, 1983). A slightly more sophisticated analysis of the temperature field inside the pedestal treats the conduction process as one dimensional and assumes a uniform heat transfer coefficient distributed over the pedestal surface. For a straight pedestal, the fin efficiency can be shown to be

$$\eta = \frac{\tanh\left(\sqrt{\frac{h}{kD}}\, H\right)}{\sqrt{\frac{h}{kD}}\, H} \tag{8}$$

where k is the pedestal conductivity. For values of the internal heat transfer coefficient and conductivity typical of engine conditions, the fin efficiency predicted by Eq. (8) can be as low as 80 percent. The effect of the nonuniform distribution of heat transfer coefficient is not so easily assessed. The measured heat transfer coefficient peaks at locations farthest from the passage wall. Since the heat flux is higher at these locations, the temperature drop through the pedestal would be expected to have a higher effect on the fin efficiency than is calculated for the uniform heat transfer coefficient case. In the present work, the temperature distribution in the pedestal and the blade wall was calculated at typical engine conditions. The cooling effect is assessed from the calculated temperature field. The accurately predicted cooling effect can then be compared with the results of the simplified calculation. A finite element analysis package was used to perform the conduction analysis. The domain in which the conduction analysis was carried out is shown in Fig. 14. A square base, one pedestal diameter thick, has been included to simulate the blade wall. On the blade internal surface, the heat transfer distribution calculated from the Nusselt number measured by the experiments was used as the exact boundary condition. At the external surface, i.e., the flat side of the base, a uniform heat transfer coefficient typical of engine values was used for all the computed cases. Typical values of the internal and external gas temperatures (510 K and 1500 K, respectively) were used in the analysis. The heat flux is assumed to be zero at all other surfaces. Calculations using averaged heat transfer coefficient over the pedestal surface were also performed for comparison. The conductivity of 25 W/mk was chosen as being typical of

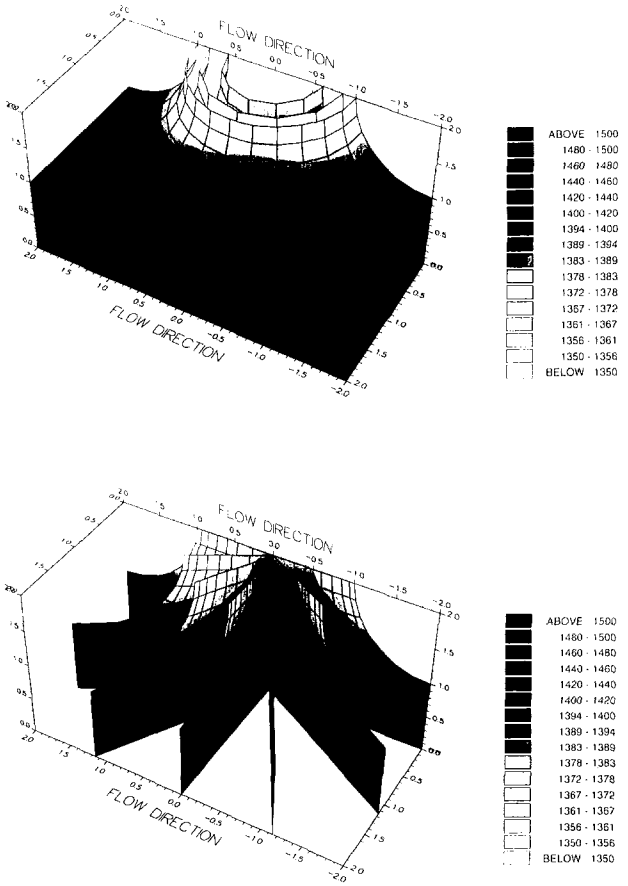

Fig. 15 Calculated temperature (in Kelvin) field for typical engine conditions

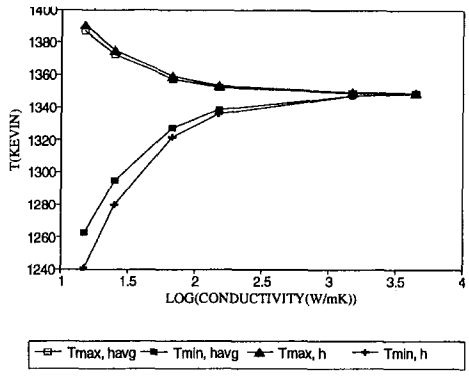

Fig. 16 Maximum and minimum temperatures

turbine blade material. The high-conductivity cases were performed to show the influence of the blade conductivity.

The computed temperature field for one set of boundary conditions is shown in Fig. 15. The lowest temperature is found, as expected, at the front facing stagnation point of the pedestal while the highest temperature is on the external (base) surface below the pedestal. Figure 16 shows the highest and lowest temperatures for both averaged and detailed heat transfer coefficients at different blade conductivities. The pedestal Reynolds number has been kept constant at 39,000. The graph shows that in this arrangement, typical of turbine cooling system, the temperature gradient across the blade is as high as 90 K at an engine representative conductivity of 25 W/Mk. It can also be seen that a lower maximum temperature and a higher minimum temperature are predicted using the averaged heat transfer coefficients. As the conductivity increases the difference disappears.

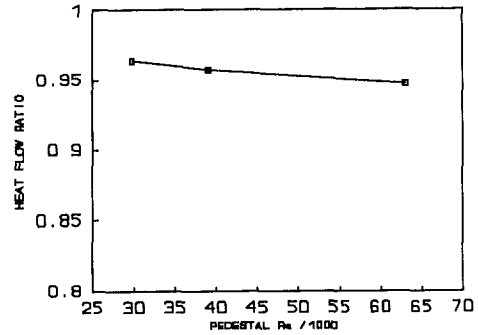

Fig. 17 Heat flow ratio for a plain wall showing only the effect of the finite blade conductivity

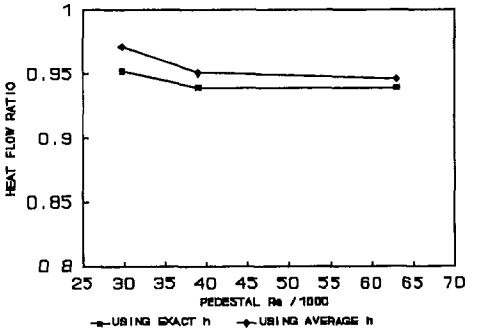

Fig. 18 Heat flow ratio as a function of pedestal Re for averaged and exact *h* distributions applied to the finite element domain

In order to evaluate the cooling efficiency of the device, the total heat flow through the square base of the pedestal for fixed gas and coolant temperatures was calculated. Since the external heat transfer coefficient is prescribed and the temperature over the face is uniform, the maximum temperature (at the base of the pedestal) is only a function of the heat flow through the device:

$$T_{\max} = T_{\text{gas}} - \frac{Q}{Ah_{\text{ext}}} \tag{9}$$

To normalize the heat flow, a base level heat flow, $Q1$, was computed for each Reynolds number. $Q1$ is the heat flow through the bottom of a $1D$ thick plate and is calculated for a conductivity of 25 W/mk when an area-weighted heat transfer coefficient boundary condition is applied at the (now) flat cooling passage wall. In other words, $Q1$ is the heat flow predicted by the simplified method, which does not account for the temperature drop through the pedestal. Before determining the exact effect of the fin efficiency, a one-dimensional approach was used to calculate the effect of the finite blade conductivity on the normalized heat flow. In the analysis used to calculate Fig. 17, the area-weighted heat transfer coefficient was applied at the inside surface of a flat wall $1D$ thick and $1D$ square. The calculated heat flow is divided by the heat flow through a $1D$ square wall of infinite conductivity. Even without simulating the effect of the extended shape of the pedestal, it can be seen that the heat flow is reduced by as much as 5 percent for the range of Reynolds numbers considered. Figure 18 compares the heat flux ratio between that predicted from the distributed heat transfer coefficient to that from the averaged heat transfer coefficient. Both the exact and the uniform average heat transfer coefficient were applied to the finite element domain. It can be seen that, when the geometry and conductivity are accurately modeled, the predicted heat flux can be lower than $Q1$ by up to 6 percent.

Conclusions

Detailed distributions of heat transfer coefficient on and around a pedestal with fillet radii have been measured using a transient heat transfer method. The distribution has been compared with previous work and it has been shown that the local heat transfer levels are significantly different to the straight cylinder case. In particular, the vortex system does not locally enhance heat transfer to the same levels measured at the root of a straight pedestal. To accurately assess the effect of the different distribution on engine metal temperatures, the exact detailed distribution was used in a conduction analysis. The influence of pedestal conductivity and the effect of the nonuniform heat transfer coefficient distribution has been quantified for typical engine conditions. It has been shown that temperature differences of about 90 K exist across the pedestal surface.

Acknowledgments

This work has been carried out with the support of the United Kingdom Ministry of Defence and Rolls-Royce plc. The technical assistance of Mr. P. J. Timms was also much appreciated. The liquid crystals were supplied by Hallcrest LCT and the finite element software was written by PAFEC Ltd.

References

Brigham, B. A., and Van Fossen, G. J., 1983, "Length to Diameter Ratio and Row Number Effects in Short Pin Fin Heat Transfer," ASME Paper No. 83-GT-138.

Byerley, A. R., Jones, T. V., and Ireland, P. T., 1992, "Internal Cooling Passage Heat Transfer Near the Entrance to a Film Cooling Hole: Experimental and Computational Results," ASME Paper No. 92-GT-241.

Chyu, M. K., 1990, "Heat Transfer and Pressure Drop for Short Pin-Fin Arrays With Pin Endwall Fillet," ASME *Journal of Heat Transfer*, Vol. 112, pp. 926–932.

Goldstein, R. J., and Karni, J., 1984, "The Effect of a Wall Boundary Layer on Local Mass Transfer From a Cylinder in Crossflow," ASME *Journal of Heat Transfer*, Vol. 106, pp. XX–OO.

Holland, M. J., 1991, "Rotor Blade Cooling in HP Turbines," Rolls-Royce report, GN30498.

Ireland, P. T., and Jones, T. V., 1986, "Detailed Measurements of Heat Transfer on and Around a Pedestal in Fully Developed Passage Flow," *Proceedings of 8th International Heat Transfer Conference*, San Francisco, pp. 975–980.

Ireland, P. T., 1987, "Internal Cooling of Turbine Blades," D.Phil Thesis, University of Oxford, United Kingdom.

Jones, T. V., Wang, Z., and Ireland, P. T., 1992, "Liquid Crystals in Aerodynamic and Heat Transfer Testing," *Proceedings of Optical Methods and Data Processing in Heat and Fluid Flow*, I.Mech.E., London.

Kays and Crawford, 1980, *Convective Heat and Mass Transfer*, 2nd ed., McGraw-Hill, New York, p. 141.

Metzger, D. E., Shepard, W. B., and Haley, S. W., 1986, "Row Resolved Heat Transfer Variations in Pin Fin Arrays Including the Effects of Non-uniform Arrays and Flow Convergence," ASME Paper No. 86-GT-132.

Shen, J.-R., Ireland, P. T., Wang, Z., and Jones, T. V., 1991, "Heat Transfer Coefficient Enhancement in a Gas Turbine Blade Cooling Passage Due to Film Cooling Holes," *Proceedings of the Institution of Mechanical Engineers, Turbomachinery*, I.Mech.E., London, pp. 219–226.

Sparrow, E. M., Stahl, T. J., and Traub, P., 1984, "Heat Transfer Adjacent to the Attached End of a Cylinder in Crossflow," *International Journal of Heat Transfer*, Vol. 27, pp. 233–242.

Van Fossen, G. J., 1982, "Heat Transfer Coefficients for Staggered Arrays of Short Pin Fins," ASME *Journal of Heat Transfer*, Vol. 104, pp. 268–274.

Wang, Z., Ireland, P. T., and Jones, T. V., 1990, "A Technique for Measuring Convective Heat Transfer at Rough Surfaces," ASME Paper No. 90-GT-300.

Wang, Z., 1991, "The Application of Thermochromic Liquid Crystals to Detailed Turbine Blade Cooling Measurements," D.Phil Thesis, University of Oxford, United Kingdom.

Zukauskas, A. A., 1972, "Heat Transfer From Tubes in Cross Flow," *Advances in Heat Transfer*, Vol. 8, pp. 116–133.